When Function Follows Form: Effects of Donor Copolymer Side Chains on Film Morphology and BHJ Solar Cell Performance

By *Jodi M. Szarko, Jianchang Guo, Yongye Liang, Byeongdu Lee, Brian S. Rolczynski, Joseph Strzalka, Tao Xu, Stephen Loser, Tobin J. Marks,* Luping Yu,** and *Lin X. Chen**

Since their discovery, organic conducting polymers have been intensely explored for a variety of potential optoelectronic applications.[1] Recently, organic photovoltaic (OPV) devices based on semiconducting polymers have emerged as attractive alternatives to inorganic solar cells due to their potential low manufacturing cost and processing flexibility. Extensive progress has been achieved in understanding OPV photophysical phenomena and in identifying key factors needed to improve organic solar cell device power conversion efficiency (PCE).[2] It was recently reported that **PTB** polymers, composed of alternating thieno[3,-*b*]thiophene and benzodithiophene units (**Figure 1a**), yield unprecedented ≈8% PCEs when blended in a bulk-heterojunction (BHJ) structure with electron acceptor materials such as [6,6]-phenyl-$C_{61(71)}$-butyric acid methyl ester (**$PC_{61}BM$** or **$PC_{71}BM$**).[3–6] Previous studies reported the synthesis of seven **PTB** polymers with the same alternating thienothiophene (**TT**) and benzodithiophene (**BDT**) backbone sequence but with varied side chains; their corresponding solar cell PCEs range from 2–8%.[7,8] The structural differences among these seven polymers arise from the aliphatic side chains appended at different backbone positions, as shown in Figure 1a. In the first **PTB** polymer of this series, **PTB1**, we discovered a remarkable "face-on" polymer backbone orientation in which the π-conjugated polymer backbone planes lie parallel to the substrate surface, resulting in maximal contacts between organic photoactive materials and the ITO anode coated with a PEDOT:PSS (poly(3,4-ethylenedioxythiophene) poly(styrenesulfonate)) interfacial layer. This orientation of the π–π stacked structures would favor charge transport across the interface.[9] In contrast, most other bulk-heterojunction (BHJ)-OPV materials, such as poly-3 hexylthiophene (**P3HT**), have a strong preference for an "edge-on" orientation, in which the π-conjugated polymer backbone planes lie nearly perpendicular to the anode surface.[10,11] The unusual orientational preference of the **PTB1** is attributed to the unique zig-zag backbone (Figure 1a), which disfavors the perpendicular orientation with respect to the substrate plane, as found for linear backbone counterparts such as **P3HT**.

The kinked **PTB1** backbone-induced packing architecture offers a fascinating new set of structural parameters to be tuned in the quest for BHJ morphologies and microstructures that maximize the device PCE. Presented here are the comparative film morphology results that were obtained for all seven of the aforementioned **PTB** polymers using grazing-incidence X-ray scattering (GIXS), along with microstructural details that reveal distinct correlations with the photovoltaic response. Grazing incident wide angle X-ray scattering (GIWAXS) is used here to characterize *d*-spacing structural features at the molecular level in both neat and BJH **PTB**-based films, while grazing incident small angle X-ray scattering (GISAXS) is used to characterize structural features with *d*-spacings on the domain size level in morphology of **PTB**:**$PC_{61}BM$** (from this point on **PCBM** will denote the **$PC_{61}BM$** fullerene) BHJ films. The GIWAXS results on these films indicate that: 1) branched side chains attached at the **BDT** unit cause an increase in the π–π stacking spacing in films and a decrease in the OPV device PCE, while branched side chains attached at the **TT** unit do not interfere with the π–π stacking spacing in the film and enhance the OPV device PCE; 2) there is a positive correlation between the strength of π–π interactions through the polymer backbone stacking in the film and the OPV device fill factor (FF), which is attributed to **PTB** interactions with the anode interfacial layer; and 3) the film fabrication with an additive 1,8-diiodooctane (**DIO**) slightly enhances the crystallinity of the polymers. From these results, we propose that the structure of the donor **PTB** polymer both inhibits long-range crystallinity and facilitates stronger donor

[*] Dr. J. M. Szarko, B. S. Rolczynski, S. Loser, Prof. T. J. Marks, Prof. L. X. Chen
Department of Chemistry
Northwestern University
Evanston, Illinois 60208 (USA)
E-mail: t-marks@northwestern.edu; lchen@anl.gov
Dr. J. M. Szarko, Dr. J. Guo, B. S. Rolczynski, Prof. L. X. Chen
Chemical Sciences and Engineering Division
Argonne National Laboratory
Argonne, Illinois 60439 (USA)
Dr. J. M. Szarko, Dr. J. Guo, B. S. Rolczynski, S. Loser, Prof. T. J. Marks, Prof. L. X. Chen
Argonne-Northwestern Solar Energy Research (ANSER) Center
Northwestern University
2145 Sheridan Road, Evanston, IL 60208 (USA)
Dr. J. Guo, Dr. Y. Liang, T. Xu, Prof. L. Yu
Department of Chemistry and The James Franck Institute
The University of Chicago
929 E 57th Street, Chicago
IL 60637 (USA)
E-mail: lupingyu@uchicago.edu
Dr. B. Lee, Dr. J. Strzalka
X-ray Science Division
Advanced Photon Source
Argonne National Laboratory
Argonne, IL 60439 (USA)

DOI: 10.1002/adma.201002687

ADVANCED MATERIALS
www.advmat.de

www.MaterialsViews.com

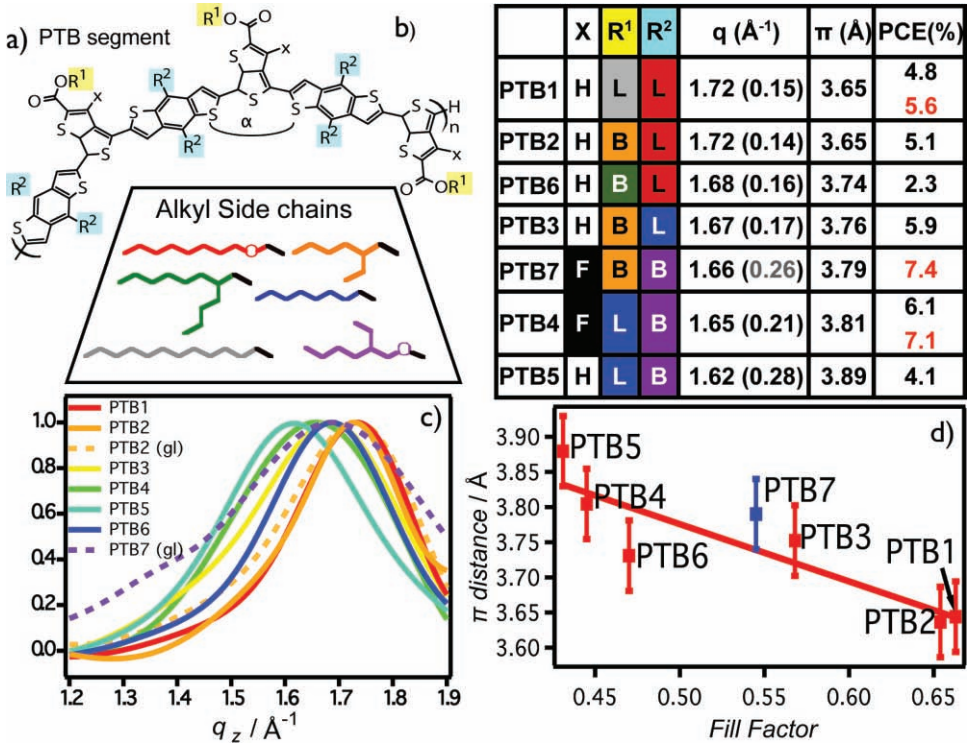

	X	R^1	R^2	q (Å^{-1})	π (Å)	PCE(%)
PTB1	H	L	L	1.72 (0.15)	3.65	4.8 5.6
PTB2	H	B	L	1.72 (0.14)	3.65	5.1
PTB6	H	B	L	1.68 (0.16)	3.74	2.3
PTB3	H	B	L	1.67 (0.17)	3.76	5.9
PTB7	F	B	B	1.66 (0.26)	3.79	7.4
PTB4	F	L	B	1.65 (0.21)	3.81	6.1 7.1
PTB5	H	L	B	1.62 (0.28)	3.89	4.1

Figure 1. a) Structure of **PTB** polymers represented by a segment representing the possible zig-zag or arched conformation the polymer backbone. The angle α is 140°. The "X" represents H or F atoms. The structures of alkyl side chains R^1 (indicated by the yellow squares) and R^2 (indicated by the blue squares) are presented in the trapezoid block. The alkyl chains are: n-octyloxy (red), 2-ethylehexyl (orange), 2-butyloctyl (green), n-octyl (blue), 2-ethylhexyloxy (violet), and n-dodecyl (grey). b) Table indicating BHJ PCE values, π–π stacking scattering vectors and linewidths (in parentheses), and π–π stacking distances for the **PTB** polymers. For more information, see the Supporting Information and Ref. [3–5]. The linear (L) or branched (B) aliphatic side chains on the **TT** and **BDT** moieties are also noted. The efficiencies in black are the recorded PCEs for BHJ films fabricated with **$PC_{61}BM$** while the efficiencies in red are for devices made with **$PC_{71}BM$**. The colored squares for R^1 and R^2 represent the side chain matching that color, which is shown to the left of the table and described in (a). c) The π–π stacking scattering vector peaks for the seven **PTB** polymers. The corresponding distances are shown (b). The solid line shows the scattering peaks for the neat films on a Si substrate while the films on a glass substrate are represented by the dotted lines. The color scheme in (c) does not correspond to the color scheme represented in panels (a) and (b). d) Correlation between OPV fill factor and the π–π stacking distance for the **PTB** polymers. **PTB7** is indicated in blue because this polymer was fabricated using **$PC_{71}BM$** while the other polymers were fabricated using **$PC_{61}BM$** in this investigation. The line is a visual aid.

and acceptor interactions in the films, thereby enhancing solar cell performance.[12,13] Thus, a new thin-film architecture strategy emerges for optimizing OPV devices.

The first focus is on correlating the GIWAXS-determined π–π stacking distances in the neat polymer films with their respective side-chain structures (Figure 1b). Representative GIWAXS scattering peaks assigned to the spacing of polymer backbone π–π stacking in neat polymer films are shown in Figure 1c. Although the fits of the scattering peaks of the neat polymers are shown for clarity, the π–π stacking distance does not vary significantly upon the addition of **PCBM** (see Supporting Information). The largest π–π stacking distance differences are found between polymers **PTB1** and **PTB5**, which can be understood from the structural differences between the aliphatic side chains attached to the **BDT** unit. Linear alkyl side chains occupy less space than branched alkyl side chains in the π–π stacking direction, resulting in a π–π stacking distance of 3.65 Å for **PTB1** versus 3.89 Å for **PTB5**. In contrast, the π–π stacking distances for **PTB1** and **PTB2** are nearly identical at 3.65 Å, although they differ in side chain structure at the **TT** backbone unit, where **PTB1** has linear alkyl side chains while **PTB2** has branched alkyl side chains. Because the **BDT** moiety has three fused heterocyclic rings with two attached side chains and is bulkier than the **TT** moiety with two fused heterocyclic rings with one attached side chain, **BDT** dominates the π–π stacking interactions. The widths of these peaks, which are also shown in Figure 1b, decrease with an increase in the scattering vector q and are inversely proportional to the domain size of the π–π stacked polymers. See Supporting Information for more details.

Next possible correlations between the π–π stacking distances in the BHJ films fabricated from these seven polymers and their OPV performance characteristics were investigated. While the **TT** unit side chains do not significantly alter the π–π stacking d-spacing, the device PCE increases substantially when the side chain is a branched alkyl group. This finding shows that the alkyl side chain attached to the **TT** unit may not affect the π–π stacking interaction significantly in this polymer series, but presumably affects **PCBM** interactions with the polymer side chains. These results complement those in Figure 1b. However, in an extreme case where very bulky side groups are attached to the **TT** unit of polymer **PTB6**, the π–π stacking distances are

substantially increased, which results in the lowest OPV device PCE. Therefore, there is a delicate interplay of **TT** side group characteristics necessary for optimum device response.

The present results also reveal a striking relationship between the OPV device FF and the π–π stacking distances of the seven **PTB** polymers, in which the closer π–π stacking distance in the polymer film gives the larger FF in its corresponding BHJ device (Figure 1d). The relationship shown here is for the devices fabricated from films under two conditions: 1) with a 1:1 weight ratio of the polymer and **PCBM** and 2) without the **DIO** additive. BHJ films of polymers **PTB1-PTB6** were fabricated using $\mathbf{PC_{61}BM}$ as the electron acceptor material while that of **PTB7** was fabricated using $\mathbf{PC_{71}BM}$. Many variables such as film morphology and film thickness are known to influence FFs in BHJ devices.[14] For the present polymer series, the FF is the electronic property that has the strongest correlation with the π–π stacking distance. Other parameters such as the short circuit current (J_{sc}) do not exhibit such a distinctive trend. This finding has implications for the nature of both the film morphology and the interaction between these donor polymers and the underlying PEDOT:PSS anode interfacial layer. The **PTB** polymers with the strongest π–π stacking have the most crystalline polymer domains and bind most strongly to the anode interfacial layer, facilitating electronic communication across the interface. Previous studies have shown that BHJ device FFs can be substantially enhanced by interfacial layers that enhance hole extraction and block undesired electron leakage.[15,16]

Next, the polymer packing structures in films are compared for the **PTB** polymers blended with **PCBM**. The respective GIWAXS results for **PTB2** and **PTB3** on silicon, both neat and blended with **PCBM**, are shown in **Figure 2a–d**. A 1:1 **PTB**:**PCBM** weight ratio was maintained in all films. The symmetric circle at the scattering vector q = 1.4 Å^{-1} in Figure 2b,d corresponds to the d-spacing from intramolecular **PCBM** distances.[17,18] The linewidth of this peak indicates that the **PCBM** domain sizes are minimally 3–4 units in length (see Supporting Information). In this medium- to wide-angle regime, all films exhibit scattering features in two regions: 1) one peak at q = 0.2–0.3 Å^{-1} (i.e., 21–31 Å d-spacing) along the horizontal y-direction and 2) multiple peaks at q = 1.6–1.8 Å^{-1} (d = 3.6–3.9 Å) along the vertical z-direction. The first peak along the y-direction corresponds to the intramolecular d-spacing distances of the polymers with extended side chains, and the second peak corresponds to an interchain π–π stacking d-spacing between polymer backbones. Because the π–π stacking distance directly influences carrier transport along the stacking directions in these films, it is physically reasonable that this distance plays an important role in the OPV device PCE. For all polymers studied here, the stacked **PTB** polymer backbone planes are parallel to the substrate, as shown by the appearance of the π–π stacking peak at $q \approx 1.6$ Å^{-1} in the z-direction. The π–π stacking distances extracted from this scattering feature are 3.65 Å for **PTB2** and 3.76 Å for **PTB3**.

It is well-recognized that the interfacial interactions between the electron donor (**PTB**) and the electron acceptor (**PCBM**) are crucial for BHJ OPV device efficiency.[1,19] Because there is no direct covalent polymer-**PCBM** bond present, numerous **PTB**-**PCBM** interfacial structural models are in principal possible. For simplification, we focus on the GIXS images such as those

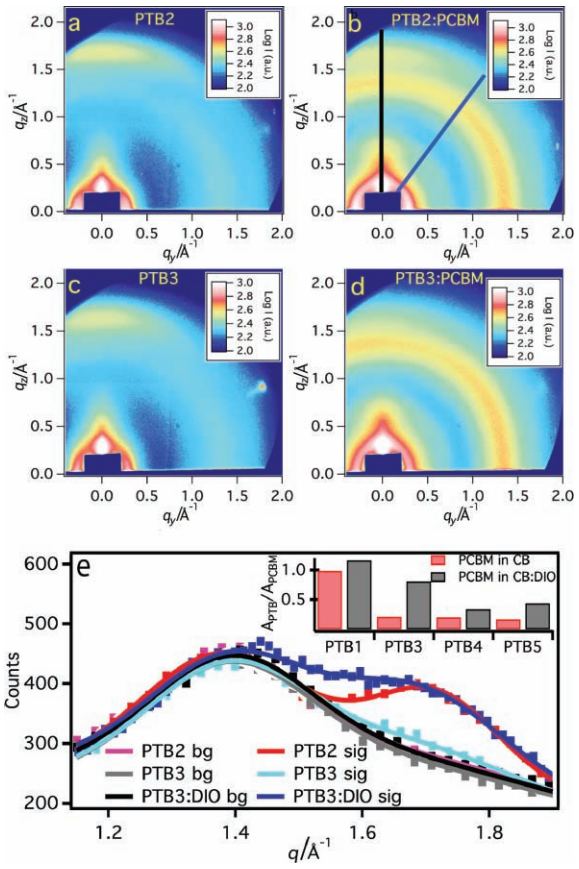

Figure 2. GIWAXS results for neat **PTB2** (a) and **PTB2** blended with **PCBM** (b). The π-stacking distance is observed in the z-direction in the neat films at a scattering vector of 1.72 Å^{-1}. The blended BHJ films exhibit a second peak at 1.4 Å^{-1} due to the **PCBM** moieties. The neat (c) and blended (d) GIWAXS results for **PTB3** show that the π-stacking interaction for this polymer is diminished when blended with **PCBM**. e) The background (blue diagonal line in (b)) and signal (black line in (b)) traces for the **PTB2:PCBM** material. A multipeak global analysis was used to fit these traces. For the signal trace, which was drawn along the z-axis, an additional peak was added for the contribution of **PTB2**. Using these fits, the ratio of the amplitude of the signal from the **PTB** and the amplitude of the **PCBM** peak, A_{PTB}/A_{PCBM}, was determined as 0.82. The polymers **PTB3**, **PTB4**, and **PTB5** were also investigated. **PTB3** is shown in Figure 2. The A_{PTB}/A_{PCBM} amplitude for **PTB3** is 0.27, indicating that the film order is disrupted due to **PCBM** partial intercalation between the polymer chains. When the films are fabricated using 3% 1,8 diiodooctane (DIO) in the solution, this ratio for **PTB** rises to 0.81. Similar trends are observed for **PTB1**, **PTB4**, and **PTB5**, which are shown in the inset of (e).

of **PTB2** and **PTB3** in Figure 2e. The anisotropic scattering features characteristic of the average d-spacing for π–π stacking in the z-direction (signal along the black line in Figure 2b) and the isotropic scattering ring in a diagonal line (background along the blue line in Figure 2b) were examined. When comparing the scattering profiles along these two directions in the scattering image, the largest contrast is observed in the **PTB2:PCBM** film. Each 1D scattering profile was fit by multiple Gaussian peaks using a global analysis procedure (see Supporting Information). The area ratio of the Gaussian peaks for the **PCBM** domain at 1.4 Å^{-1} (A_{PCBM}) and the polymer π-π stacking at ≈1.7 Å^{-1} (A_{PTB}) was used to characterize the degree of polymer packing order in the films. For the **PTB2:PCBM** film, the ratio

$(A_{PTB})/(A_{PCBM})$ = 0.51. In contrast, $(A_{PTB})/(A_{PCBM})$ = 0.20 for the **PTB3**:**PCBM** film. This finding indicates that **PCBM** disrupts the π–π stacking in **PTB3**:**PCBM** films more effectively than in **PTB2**:**PCBM** films. This result agrees with the observed closer π–π stacking distance and smaller linewidths in the neat **PTB2** films, corresponding to a stronger inter-backbone interaction. Consequently, the **PCBM** molecules encounter a higher intercalation energy barrier in **PTB2** versus **PTB3**. The crystallinity of all the **PTB** polymers is also lower compared to more conventional OPV polymers such as **P3HT**, which implies that the **PCBM** molecules can penetrate through the **PTB** domains more easily.

The **PTB**:**PCBM** films with **PTB1**, **PTB3**, **PTB4**, and **PTB5** as the donors exhibit higher PCEs when prepared with the processing additive 1,8 diiodooctane (DIO).[20,21] As an example, the corresponding GIWAXS data for **PTB3**:**PCBM** films prepared in presence of 3% DIO in the solution (Figure 2e) gives the ratio $(A_{PTB})/(A_{PCBM})$ = 0.62. Comparing this value with the aforementioned $(A_{PTB})/(A_{PCBM})$ = 0.20 for the **PTB3**:**PCBM** films, the relative peak area corresponding to the π–π stacking domains in the films prepared with DIO is enhanced by a factor of 3, resulting from greater polymer crystallinity in the latter. The $(A_{PTB})/(A_{PCBM})$ ratios for polymer:PCBM films with **PTB3**, **PTB4**, and **PTB5** are shown in the inset of Figure 2e. The effects of DIO on the π–π stacking in the **PTB4** and **PTB5** films are significant but smaller, while the effect for **PTB1** is the smallest due to the stronger π–π stacking interactions in this material. Although DIO enhances the π–π stacking domains in all of the present films, the **PTB2**:**PCBM** films still have the strongest π-stacking domains without the DIO addition, yet do not exhibit particularly striking PCEs. This result suggests interplay between optimal π–π stacking for exciton diffusion and optimal PCBM intercalation for optimal electron-hole separation.

Finally, the long range morphology of the **PTB** BHJ films was investigated by the GISAXS measurements. The results for **PTB6**:**PCBM**, **PTB3**:**PCBM**, and **P3HT**:**PCBM** films on silicon substrates are shown in **Figure 3**a. **PTB6** was chosen for comparison because it has the largest electron density difference versus **PCBM** (see Supporting Information) and similar results were obtained for all of the **PTB** polymers. In contrast to the GIWAXS results, the GISAXS results do not have distinctive patterns, but only the lineshapes provide information on the film domain dimensions. For the **P3HT**:**PCBM** film, the average **P3HT** and **PCBM** domain dimension is 5–10 nm as shown by the form factor extracted from a "Guinier knee" in this *q*-region (Figure 3a).[20] In contrast, the **PTB6** and **PTB3** films do not exhibit a large feature in the form factor. No intermolecular interactions or peaks from the **PCBM** are observed in this region, which further indicates that the **PCBM** is well incorporated in the system. Since the electron density of **PTB6** is similar to that of **P3HT** (see Supporting Information), electron density differences are not responsible for the present form factor differences. This finding does not indicate that the **PCBM** molecules are completely separated and intercalated into the polymer system as was reported in previous systems.[22] Instead, this information indicates that the **PCBM** domain sizes are smaller in **PTB**:**PCBM** films compared to the **P3HT**:**PCBM** films. A proposed schematic of the BHJ film structure is shown in Figure 3b, which is derived from the observed trends in both

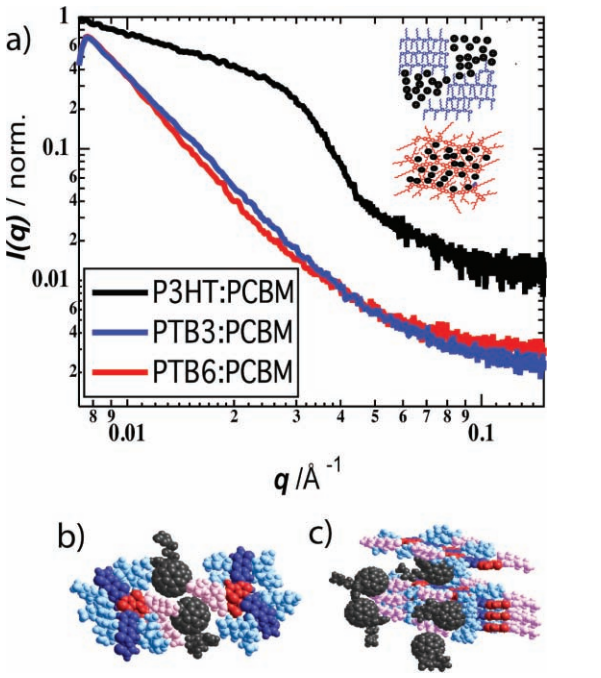

Figure 3. The GISAXS line trace for **PTB6** and **PTB3** blended films. All PTB polymers had similar linetraces. For comparison, the same information for **P3HT**-blended film is shown. This information, along with the GIWAXS results, indicates that the **PCBM** is intertwined in between the polymer chains. In the inset, a rough schematic of the top view of the **P3HT** (blue lines, top) and **PCBM** (black lines) film is shown (top) along with the **PTB** (red lines) and **PCBM** (black lines) (bottom). The **PTB** films do not show the longer range order that has been observed in the **P3HT** films. The proposed **PCBM** interaction with the **PTB** polymer chains is shown in more detail in (b) and (c). The red components are the **TT** units and the dark blue components are the **BDT** units. The pink units are the aliphatic chains on **TT** while the light blue units are the aliphatic chains on **BDT.** The **PCBM** molecule are shown in black. Panel (b) shows a cut of the interaction of **PCBM** between two polymer chains while (c) shows the side-view proposed orientation of **PCBM**. The **PCBM** molecules may have a slight preference to orientate around the aliphatic side chains of the **TT** units. Some of the **PCBM** molecules can also disrupt the π–π stacking of the polymer domains. The extent of this disruption depends on the intermolecular forces in the π bond.

the small and wide angle data. The **PCBM** penetrates through the weak **PTB** crystal domains and forms a network of small fibrous domains through the film. It is more likely for **PCBM** to penetrate the π–π stacking of the **PTB** domains near the **TT** unit than the **BDT** unit because the latter has an extended three-ring structure with stronger π–π interactions with conjugated backbones.

In conclusion, the grazing incident X-ray scattering information on seven related OPV **PTB** donor polymer films is presented. The GIWAXS results show that film morphology is very sensitive to the structure of the **PTB** side groups attached to the **TT** or **BDT** subunits. Differences in how the structure depends on the subunit side groups are attributed to both π–π stacking interactions in the polymer domains and **PCBM** incorporation into these domains. The GISAXS data show that the **PCBM** domains with tens of nanometers dimensions, typically present in most BHJ OPV films, are not present in these **PTB**-based

materials. Together, these results indicate that the materials architecture of **PTB**-based OPV devices has a completely new structural foundation, which in turn creates a very different BHJ morphology/microstructure. Subtle changes in the electronic and side-chain structures in this framework should lead to a large, informative data set for optimizing structure and OPV efficiency.

Supporting Information

Supporting Information, including device fabrication, X-ray fitting analysis, X-ray reflectivity, solar cell parameters, and other experimental details, is available from the Wiley Online Library or from the author.

Acknowledgements

This research is supported by the ANSER Center, an Energy Frontier Research Center funded by the U.S. Department of Energy, Office of Science, Office of Basic Energy Sciences, under Award Number DE-SC0001059, and the Division of Chemical Sciences, Office of Basic Energy Sciences, the U.S. Department of Energy under contract DE-AC02–06CH11357 (for L.X.C.). The synthesis of polymers is also supported by the National Science Foundation, AFOSR, and the NSF MRSEC program at the University of Chicago (L.Y.). The authors would also like to thank Sonke Seifert for help with the X-ray scattering experiments.

Received: July 27, 2010
Revised: September 1, 2010
Published online:

[1] a) E. B. Namdas, M. Tong, P. Ledochowitsch, S. R. Mednick, J. D. Yuen, D. Moses, A. J. Heeger, *Adv. Mater.* **2009**, *21*, 799; b) H. Sirringhaus, M. Ando, *MRS Bull.* **2008**, *33*, 676; c) H. Klauk, *Organic Electronics: Materials, Manufacturing, and Applications*, Wiley-VCH, Weinheim, Germany, **2006**.

[2] a) G. Dennler, M. C. Scharber, C. J. Brabec, *Adv. Mater.* **2009**, *21*, 1323; b) P. Heremans, D. Cheyns, B. P. Rand, *Acc. Chem. Res.* **2009**, *42*, 1740; c) S. H. Park, A. Roy, S. Beaupré, S. Cho, S. Coates, J. S. Moon, D. Moses, M. Leclerc, K. Lee, A. J. Heeger, *Nat. Photonics*, **2009**, *3*, 297.

[3] Y. Y. Liang, Z. Xu, J. Xia, S. T. Tsai, Y. Wu, G. Li, C. Ray, L. P. Yu, *Adv. Mater.* **2010**, *22*, E135.

[4] Y. Y. Liang, Y. Wu, D. Q. Feng, S. T. Tsai, H. J. Son, G. Li, L. P Yu, *J. Am. Chem. Soc.* **2009**, *131*, 56.

[5] Y. Y. Liang, D. Q. Feng, Y. Wu, S. T. Tsai, G. Li, C. Ray, L. P. Yu, *J. Am. Chem. Soc.* **2009**, *131*, 7792.

[6] H. Y. Chen, J. H. Hou, S. Q Zhang, Y. Y. Liang, G. W. Yang, Y. Yang, L. P. Yu, Y. Wu, Y. G. Li, *Nat. Photonics* **2009**, *3*, 649.

[7] C. Piliego, T. W. Holcombe, J. D. Douglas, C. H. Woo, P. M. Beaujuge, J. M. J. Frechet, *J. Am. Chem. Soc.* **2010**, *132*, 7595.

[8] A. P. Zoombelt, M. A. M. Leenen, M. Fonrodona, Y. Nicolas, M. M. Wienk, R. A. J. Janssen, *Polymer* **2009**, *50*, 4564.

[9] J. C. Guo, Y. Y. Liang, J. Szarko, B. Lee, H. J. Son, B. S. Rolczynski, L. P. Yu, L. X. Chen, *J. Phys. Chem. B* **2010**, *114*, 742.

[10] H. H. Yang, S. W. LeFevre, C. Y. Ryu, Z. N. Bao, *Appl. Phys. Lett.* **2007**, *90*, 172116.

[11] C. W. Chu, H. C. Yang, W. J. Hou, J. S. Huang, G. Li, Y. Yang, *Appl. Phys. Lett.* **2008**, *92*, 103306.

[12] N. C. Cates, R. Gysel, J. E. P. Dahl, A. Sellinger, M. D. McGehee, *Chem. Mater.* **2010**, *22*, 3543.

[13] N. C. Cates, R. Gysel, Z. Beiley, C. E. Miller, M. F. Toney, M. Heeney, I. McCulloch, M. D. McGehee, *Nano Lett.* **2009**, *9*, 4153.

[14] M. Kim, B. Kim, J. Kim, *ACS. Appl. Mater. Interfaces* **2009**, *1*, 1264.

[15] a) A. W. Hains, C. Ramanan, M. D. Irwin, J. Liu, M. R. Wasielewski, T. J. Marks, *ACS Appl. Mater. Interfaces* **2010**, *2*, 175; b) A. W. Hains, J. Liu, A. B. F. Martinson, M. D. Irwin, T. J. Marks, *Adv. Funct. Mater.* **2010**, *20*, 595; c) M. D. Irwin, B. Buchholz, A. W. Hains, R. P. H. Chang, T. J. Marks, *Proc. Natl. Acad. Sci. USA* **2008**, *105*, 2783.

[16] V. Djara, J. C. Bernede, *Thin Solid Films* **2005**, *493*, 273.

[17] M. Y. Chiu, U. S. Jeng, C. H. Su, K. S. Liang, K. H. Wei, *Adv. Mater.* **2008**, *20*, 2573.

[18] M. Morana, M. Wegscheider, A. Bonanni, N. Kopidakis, S. Shaheen, M. Scharber, Z. Zhu, D. Waller, R. Gaudiana, C. Brabec, *Adv. Funct. Mater.* **2008**, *18*, 1757.

[19] Xin, O. G. Reid, G. Q. Ren, F. S. Kim, D. S. Ginger, S. A. Jenekhe, *ACS Nano* **2010**, *4*, 1861.

[20] J. K. Lee, W. L. Ma, C. J. Brabec, J. Yuen, J. S. Moon, J. Y. Kim, K. Lee, G. C. Bazan, A. J. Heeger, *J. Am. Chem. Soc.* **2008**, *130*, 3619.

[21] F. Padinger, R. S. Rittberger, N. S. Sariciftci, *Adv. Funct. Mater.* **2003**, *13*, 85.

[22] A. C. Mayer, M. F. Toney, S. R. Scully, J. Rivnay, C. J. Brabec, M. Scharber, M. Koppe, M. Heeney, I. McCulloch, M. D. McGehee, *Adv. Funct. Mater.* **2009**, *19*, 1173.